Measurement of the radiative cooling rates for high-ionization species of krypton using an electron beam ion trap

R. Radtke, C. Biedermann, T. Fuchs, and G. Fußmann
Max-Planck-Institut für Plasmaphysik, Bereich Plasmadiagnostik, EURATOM Association, D-10117 Berlin, Germany

P. Beiersdorfer
University of California, Lawrence Livermore National Laboratory, Livermore, California 94550
(Received 18 June 1999)

We describe a measurement of the radiative cooling rate for krypton made at the Berlin electron beam ion trap (EBIT). The EBIT was tuned to a charge-state distribution approaching the ionization balance of a plasma at a temperature of about 5 keV. To determine the cooling rate, we made use of EBIT's capabilities to sample a wide range of electron-beam energies and distinguish between different radiation channels. We have measured the x-ray emission from bremsstrahlung, radiative recombination, dielectronic recombination, and line radiation following electron-impact excitation. The dominant contribution to the cooling rate is made by the $n=3-2$, $n=4-2$, ... x rays of the L-shell spectra of krypton, which produce more than 75% of the total radiation loss. A difference with theoretical calculations is noted for the measured total cooling rate. The predicted values are lower by a factor of $1.5-2$, depending on the theoretical model. For our measurement of the cooling rate, we estimate an uncertainty interval of $22-30\,\%$.

PACS number(s): 52.25.Nr, 32.30.Rj, 34.80.Lx, 34.80.Kw

I. INTRODUCTION

For the future large tokamaks, such as the International Thermonuclear Experimental Reactor (ITER), control of the energy release from the plasma is among the most critical issues for successful operation. Estimates and modeling calculations show that, for ITER conditions, neutral hydrogen losses are not large enough to limit the heat load on the plasma-facing components to technically tolerable values [1]. Thus, additional radiation losses from impurities are required, ideally resulting from precisely controlled admixtures of recycling gases. In the search for an appropriate candidate for cooling purposes, krypton has been recently proposed because it is expected to provide radiative cooling of the edge region at a rate of the order of 100 MW without perturbing the core of the ITER plasma [2]. First results from krypton experiments at the Tokamak Fusion Test Reactor (TFTR) have demonstrated the success of radiative cooling in decreasing both the electron temperature and density of the edge plasma [3,4]. In a recent study at the TFTR, controlled krypton puffing was used for heat dispersal showing that, at reactor-plasma conditions, a substantial portion of the input power (up to 75%) can be exhausted by radiation [5]. Also, the confinement of the plasma and the integrated fusion power was improved in these experiments relative to the levels without krypton injection.

In addition, for ITER plasmas, krypton is also considered a promising candidate for x-ray diagnostic measurements to determine the central ion temperature [3,6]. The electron temperatures in ITER plasmas are expected to be in the range of 10–30 keV. Unlike lower-Z elements, such as Fe and Ni used on present-day tokamaks, krypton will not be fully stripped in the hot plasma core, so that its K-shell radiation can still be observed under such high-temperature plasma conditions. From our ionization-equilibrium calculations, for example, we infer that H-like Kr^{35+} and He-like Kr^{34+} are the dominant charge states for electron temperatures T_e from 10 to 30 keV contributing more than 70% to all of the ionized krypton atoms.

For the understanding and modeling of the effects of injecting krypton into tokamak plasmas, knowledge of the atomic physics data for all of the ion species encountered in the plasma is required. The main interest at the present time is in the radiative cooling rates, which are needed to predict the power radiated from the high charge states of krypton. Relating to calculated cooling rates, the most extended results are given in Ref. [7] where 47 elements, including krypton, were treated within the framework of the average-ion model. A more recent *ab initio* calculation for mid- and high-Z elements was performed in [8] using the multiconfiguration relativistic Hebrew University Lawrence Livermore Atomic Code (HULLAC) package. The results for krypton show major discrepancies with the previous calculations [7], but provided a much better agreement with a recent experiment [9] where the cooling rates were measured at the Frascati Tokamak Upgrade (FTU) as a function of T_e ranging from 0.1 to 1.7 keV. In order to extend the cooling rates to the high-temperature conditions of future tokamaks measurements are required employing yet other experimental techniques.

In this paper, we describe a measurement of the radiative cooling rates for high-ionization species of krypton at the Berlin electron beam ion trap (EBIT) facility. EBIT uses a nearly monoenergetic, magnetically compressed electron beam for the excitation of the ions and has the advantage over hot plasmas that specific electron-ion interactions can be easily identified in an EBIT spectrum. The appropriate technique for observing the radiation from the ions in EBIT is to create a particular ion population at one energy and then probe the ions by fast scans of the beam energy. For the present investigation, we have tuned the EBIT to an ion population approaching the ionization balance of a plasma at

an electron temperature of about 5 keV. The preselected ion population was sampled by linear sweeps of the beam energy extending from about 1 to 25 keV. This is the proper range to generate the *K*-shell, *L*-shell, and *M*-shell spectra of the highly charged krypton ions as well as to excite *K*Ln and *L*Mn ($n=2,3,\ldots$) dielectronic resonances. We determined the radiative cooling rates by measuring the x-ray emission as a function of both the beam energy and x-ray energy, normalizing the measurements relative to the intensity of photons from radiative recombination at a fixed reference energy, generating spectra of x-ray intensity versus beam energy for the different radiation processes and taking the Maxwellian average corresponding to the value specified for T_e. Unlike previous experiments on tokamak plasmas, our EBIT measurement can distinguish between the different radiation channels that contribute to the cooling rates. Moreover, the abundance of impurity ions in a tokamak plasma is influenced by radial transport, and it is difficult to separate transport processes from atomic processes in the study of the radiation from impurity ions. In addition, the spectra from tokamak plasmas are averaged over a range of electron temperatures and densities and require inversion into local emission coefficients using routines of established accuracy. The present measurements avoid these experimental difficulties.

The paper is organized as follows. First, in Sec. II, we outline the plasmaphysical background of the present investigation and explain the experimental approach used for measuring radiative cooling rates. In Sec. III, we focus on the experimental setup at the EBIT device, and in Sec. IV we present the results of our measurements. In Sec. V, we give the radiative cooling rates and make a comparison with theoretical predictions. Finally, in Sec. VI, we summarize the results and draw conclusions.

II. THEORETICAL CONSIDERATIONS AND METHOD

A useful approximation to describe the ionization structure and the radiation of impurity ions confined in low-density, high-temperature plasmas is the steady state coronal equilibrium model. According to this model, the number densities of two adjacent charge states are related through the balance between the ionization and recombination rates, i.e.,

$$n_{Z,q}S_{Z,q}=n_{Z,q+1}R_{Z,q+1}, \tag{1}$$

where $S_{Z,q}$ is the ionization-rate coefficient from the ion of charge state q to charge state $q+1$, and $R_{Z,q+1}$ is the recombination-rate coefficient from the ion of charge state $q+1$ to charge state q. Z designates the nuclear charge of the ion species ($Z=36$ for krypton). $R_{Z,q+1}$ in Eq. (1) is due to both radiative and dielectronic recombination, and we point out that the radiative recombination rates drop rapidly with increasing temperature causing dielectronic recombination to become increasingly important under tokamak plasma conditions. In the coronal approximation, the specific power $P_{\rm rad}$ radiated by the impurity ions is given by

$$P_{\rm rad}=n_e n_Z L_Z(T_e). \tag{2}$$

Here, n_e is the electron density, $n_Z=\Sigma_q n_{Z,q}$ is the total density of the atomic species Z, and $L_Z(T_e)$ is the cooling rate (sometimes this quantity is called radiation function). The cooling rate is a function only of the electron temperature T_e and gives the energy loss per free electron and per ion produced by all radiative processes. For the calculation of $L_Z(T_e)$, account has to be taken for the contributions from bremsstrahlung, radiative recombination (RR), line radiation following impact excitation (IE) by electrons, and dielectronic recombination (DR). We can use the fractional abundances of the ion charge states $x_{Z,q}(T_e)=n_{Z,q}/n_Z$, where $\Sigma_q x_{Z,q}(T_e)=1$, and express $L_Z(T_e)$ as

$$L_Z(T_e)=\sum_q x_{Z,q}(T_e)L_{Z,q}(T_e), \tag{3}$$

showing that $L_Z(T_e)$ is obtained as weighted sum of the rates for all ions. There is of course a large number of expressions in the literature allowing to generate theoretical rates for different species with all degrees of ionizations needed (see, e.g., Refs. [7] and [10]). However, because of the uncertainties of many of the input atomic data, the rates are of varying degrees of reliability, often not accurate to better than a factor of two. We thus refrain from giving detailed rate formulas here, but emphasize the general expression defining the cooling rate for a plasma:

$$L_{Z,q}(T_e)=\int_0^\infty \langle v_e\sigma_{\rm rad}\rangle_{h\nu}\, d(h\nu), \tag{4}$$

where

$$\langle v_e\sigma_{\rm rad}\rangle_{h\nu}\equiv\sum_\kappa \int_0^\infty \sqrt{2E/m_e}\,\sigma_{{\rm rad},\kappa}(Z,q,E,h\nu)\, f_e(E,T_e)\, dE. \tag{5}$$

Here, $f_e(E,T_e)$ is the distribution of the electron energies, which is assumed to be Maxwellian, h is the Planck constant, and m_e, v_e, and E are the electron's mass, velocity, and energy, respectively. $\sigma_{{\rm rad},\kappa}(Z,q,E,h\nu)$ is the cross section for the specific electron-ion interaction ($\kappa=$ IE, RR, etc.), and $h\nu$ is the energy of the photon emitted as a result of the collision process. If other transitions besides single-step radiative decay are possible, the cross section in Eq. (5) is to be summed over the various decay channels, with the appropriate branching ratios as weight factors. In particular, this is necessary if higher-energy levels are populated by IE or if electron capture into high-n shells takes place in the course of radiative or dielectronic recombination.

We turn now to the description of the technique used to determine radiative cooling rates from x-ray measurements involving the EBIT apparatus. For simplicity, we first neglect the effects of the nonisotropic x-ray emission in EBIT, although we make corrections for them in the final analysis. As already mentioned, the measurement scheme is based on a steady-state ion population, which is probed by fast scans of the beam energy. Let Λ represent the set of all the EBIT operating parameters that govern the ion population in steady state. Then, when scanning this population by sweeping the beam energy E, the rate at which photons of energy $h\nu$ are radiated from the trap into the solid angle $\Delta\Omega$ is given by

$$I_{h\nu}(E)=\frac{j_e}{e}N_Z(\Lambda)\frac{\Delta\Omega}{4\pi}\sum_{\kappa}\sum_{q}\overline{x}_{Z,q}(\Lambda)\,\sigma_{\mathrm{rad},\kappa}(Z,q,E,h\nu). \tag{6}$$

Here, j_e is the effective current density of the electron beam, which is fixed in the present experiment, and e is the charge of the electron. $N_Z(\Lambda)$ is the total number of ions in the beam and $\overline{x}_{Z,q}(\Lambda)$ is the fractional abundance of the ion in charge state q averaged over the beam volume. Again, the sum over κ represents the combined effects of all possible electron-ion interactions, with $\sigma_{rad,\kappa}(Z,q,E,h\nu)$ the corresponding cross sections. It is important to stress that this EBIT experiment enables us to obtain the $\overline{x}_{Z,q}(\Lambda)$ from x-ray spectroscopic measurements. A description of the measurement scheme is given in Sec. III. Unfortunately, there is no reliable way to determine the number of ions $N_Z(\Lambda)$ and the effective current density j_e. However, instead the combined factor F, where

$$F=\frac{j_e}{e}N_Z(\Lambda)\frac{\Delta\Omega}{4\pi}, \tag{7}$$

can be obtained in the course of the normalization procedure and $\overline{x}_{Z,q}(\Lambda)$ determination. $\Delta\Omega$ in Eq. (7) is the solid angle subtended by the solid-state detector used for the x-ray measurements; $\Delta\Omega/4\pi\approx 3.8\times 10^{-4}$ in our experiment. If we scan the ions over a large energy range ($E_{\min}\ll kT_e\ll E_{\max}$) and record at the same time the x-ray spectrum emitted during the scans, then it is possible to integrate $I_{h\nu}(E)$ over both the beam energy and photon energy and evaluate the following quantity:

$$L_Z(\Lambda,T_e)=\frac{1}{F}\int_0^\infty\int_0^\infty\sqrt{2E/m_e}I_{h\nu}(E)\,f_e(E,T_e)\,dE\,d(h\nu). \tag{8}$$

For conditions where the steady-state ion population in EBIT approaches the ionization balance of a plasma, i.e., for

$$\overline{x}_{Z,q}(\Lambda)\approx x_{Z,q}(T_e), \tag{9}$$

Eq. (8) is a function only of the electron temperature and corresponds to the expression for the radiative cooling rate given by Eq. (3). Equations (8) and (9) form the basis for the measurements presented in this paper. We note that, in an EBIT experiment, a scatter plot of x-ray energy versus electron-beam energy can be created for the x rays observed permitting to isolate specific electron-ion interactions [indicated by different indices κ in Eqs. (5) and (6)].

It is worth stressing that, in practice, it is not necessary to carry out the E and $h\nu$ integrations in Eq. (8) from zero to infinity. The reason is that, for the krypton ions of present interest (C-like Kr^{30+} to He-like Kr^{34+}), the overwhelming contribution to the cooling rate is made by the radiation in the x-ray region above roughly 500 eV. Further, there is a constraint in the integration over E because the effect of $\sqrt{E}f_e(E,T_e)$, the weight function in Eq. (8), is significant only in a fairly limited energy interval, depending on the value specified for T_e.

III. EXPERIMENTAL SETUP

EBIT employs an electron beam to produce, confine, and excite highly charged ions. The electron beam is formed by accelerating and guiding electrons from an electron gun into the trap region, consisting of an assembly of three drift tubes. As the electrons pass through the trap region, the beam is compressed to a diameter of about 70 μm by a 3-T magnetic field. Atoms injected into the trap are successively ionized and radially confined by the space charge of the electron beam. Axial confinement is provided within a 2-cm-long trapping region by the two end-drift tubes, which are biased positive with respect to the center-drift tube. For the present measurements, neutral krypton atoms were continuously fed into the trap from a differentially pumped gas injector and ionized by a 26-mA-current electron beam. The relatively low electron current was used to fulfil the requirements for the EBIT operating with low voltages applied to the drift tubes.

The x rays were observed at 90° to the beam direction using a solid-state Ge detector. The detector is coupled to the same vacuum as the EBIT and operates windowless to extend the spectra down to the sub-keV x-ray range. Further, the receiver of the detector is moved closer to the trapping region (minimum distance from the EBIT center: 7 cm) allowing to collect photons in a larger solid angle.

The experiment was performed in several steps. At first, the fractional abundances of the highly charged krypton ions were determined from the *KLL* dielectronic-excitation spectrum following the procedure described in Ref. [11]. In essence, the method consists of finding the best fit between the measured and predicted DR excitation spectrum where the charge-state balance and the electron-beam energy width are the fitted parameters. To measure the *KLL* resonance for the trapped ions, we used the same data acquisition setup and similar voltage and timing patterns as in Ref. [11]. In our measurement scheme, the ions were probed 3 s after closing the trap by switching the electron-beam energy from the ionization energy ($E_{\mathrm{ion}}=10.5$ keV) to 8.6 keV and then sweeping it within 20 ms through the *KLL* resonance (1.5 keV sweep interval, 75 eV/ms sweep rate). This switch-sweep procedure was repeated every 120 ms for a period of about 0.6 s, after which the trap inventory was dumped to prevent the accumulation of high-Z background ions. During the sweeps, the beam energy and the x-ray energy for each x ray detected with the solid-state detector were recorded. The probe and dump sequence was repeated many times, with the data from each scan being added to the previous scans.

We made measurements on the *KLL* resonance of krypton at several different run conditions of EBIT, and the data were analyzed in terms of the charge-state abundances for krypton. The results were then compared with the ion abundances obtained from our ionization-equilibrium calculations (see Sec. IV). In this way, we could tune EBIT's performance aiming for a charge-state distribution which resembles the ionization balance of a plasma. To control the charge-state abundances in EBIT, we used the ionization energy and time, the axial trap depth, and the pressure in the gas injector as parameters.

Having optimized EBIT, in the main experiment we then probe the particular charge-state distribution of trapped ions

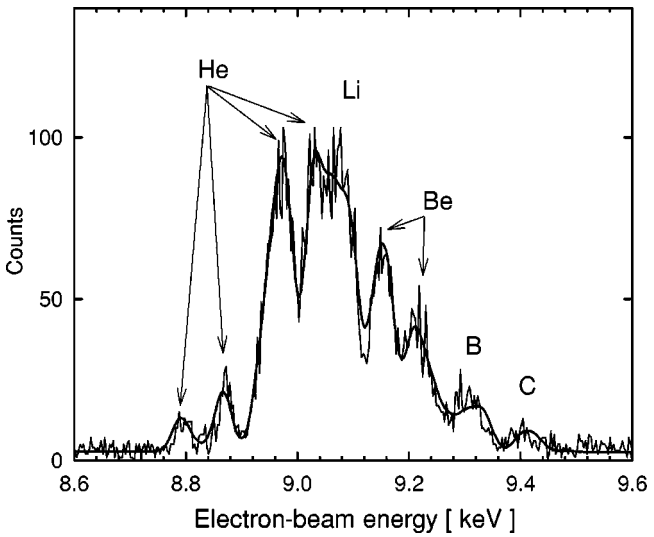

FIG. 1. Experimental (thin line) and theoretical (thick line) DR excitation spectrum for the *KLL* resonance of krypton target ions. The features labeled He, Li, Be, B, and C are the signatures of the corresponding ionic state of krypton in the excitation spectrum. The fractional ion abundances determined through the fitting process are given in Table I. The Gaussian beam-energy width that provides a match to the observed spectrum is 36 eV full width at half maximum.

by sweeping the electron-beam energy over a wide range of energy values while observing the intensities of the emitted x rays. We used the same timing cycle to control EBIT as for the *KLL* resonance measurements, with the only exception that the voltage levels were now extended from 0.9 to 25 kV during the 20-ms probing (1.2 keV/ms sweep rate). At the low end of the scan, the interval is limited by the fact that we had to maintain a constant electron current throughout the entire probing. Reducing the voltage below 0.9 keV would have required a substantial reduction of the electron current such that the rate at which photons are produced would have been intolerably small. At the high end, we have limited the beam-accelerating voltage to 25 kV to avoid electric breakdowns and ensure safe operation of the EBIT over the whole run time. The impact of these restrictions on the determination of the radiative cooling rates will be discussed in Secs. IV and V. In order to acquire adequate statistics, spectra were generated from data recorded over a period of about 60 h.

IV. MEASUREMENTS AND ANALYSIS

A. Fractional ion abundances

The measurement of the fractional abundances of the highly charged krypton ions was based on the x-ray spectrum taken with the electron-beam energy swept over the *KLL* dielectronic resonance. In the DR process via the *KLL* resonance, electron capture of a free electron into the *L* shell and concurrent excitation of the 1*s* electron to the *L* shell (or vice versa) takes place. If the recombined ion decays to a nonautoionizing state by the emission of a stabilizing photon ($n=2-1$ transition), the DR process is complete. Figure 1 shows the DR spectrum for the particular ion population we selected for the measurement of the radiative cooling rates.

TABLE I. Fractional abundances (in %) of the krypton ion-charge states: $x(\Lambda)$ represents the abundances obtained from the fit of the experimental and theoretical DR excitation spectrum (Fig. 1); $x(T_e)$ represents the predictions from the steady state coronal equilibrium model with $kT_e=4.7$ keV. Note that, for the $x(T_e)$ distribution, C-like to He-like charge states of krypton account for more than 97% of the total ion population. The average ionic charge, $\langle q\rangle=\Sigma_i q_i x_i$, for the $x(\Lambda)$ and $x(T_e)$ distributions is 32.7 and 32.5, respectively. $\Delta=|x(\Lambda)-x(T_e)|$ is the fractional difference between the measured and fitted values of the ion abundance expressed as a percentage.

Ion	$x(\Lambda)$	$x(T_e)$	Δ
H-like Kr^{35+}	0.0	0.4	0.4
He-like Kr^{34+}	33.2	34.8	1.6
Li-like Kr^{33+}	27.3	21.8	5.5
Be-like Kr^{32+}	20.0	21.9	1.9
B-like Kr^{31+}	13.0	13.2	0.2
C-like Kr^{30+}	6.5	5.6	0.9
N-like Kr^{29+}	0.0	1.8	1.8

(Aiming for this ion population led to the following operating parameters of EBIT: ionization-beam energy $E_{\text{beam}}=10.5$ keV, ionization time $\tau_{\text{ion}}=3$ s, axial trap depth $V_{\text{axial}}=100$ V, pressure in the gas injector $p_{\text{gas}}=2.7\times10^{-6}$ Pa). In addition, the theoretical DR spectrum resulting from the fit process is given in Fig. 1. For the details on the data analysis and fit procedure see Ref. [11]. Only the results of the analysis are presented here. As indicated in Fig. 1, up to five charge states could be resolved in the dielectronic-recombination spectrum. The highest charge state is He-like Kr^{34+} in accordance with the fact that we have set the electron-beam energy to a value below the ionization potential for this ion (17.3 keV). The high-energy shoulder of the resonance spectrum shows that, in addition, Li-, Be-, B-, and C-like krypton ions were detected in the trap. The counts, which appear in the DR spectrum as background, originate from nonresonant radiative recombination events of electrons onto the $n=2$ shell of krypton ions. Table I displays, for the respective charge states, the fractional abundance determined through the fitting process. It is seen that they increase gradually with increasing charge state, but do not exhibit a substantially enhanced maximum for the He-like Kr^{34+}.

In order to compare the $x(\Lambda)$ distribution to the ionization balance of a plasma, we have calculated fractional ion abundances as a function of the electron temperature taking the relation Eq. (1) as the basis. For the ionization-rate coefficients we used the formula proposed by Lotz [12], with the ionization potentials and binding energies calculated with the GRASP[2] code [16]. The rate coefficients for radiative recombination and dielectronic recombination were calculated using the empirical rate formulas by Kim and Pratt [13] and by Hahn [14,15], respectively. We mention in this context that the predictions from the rate formulas for dielectronic recombination agree with the results of our recent DR measurements [11] to within 12%. Based on these rate coefficients, Fig. 2 shows the charge balance for electron temperatures ranging from 1 to 100 keV. Note in Fig. 2 that the charge states between Ne-like Kr^{26+} and He-like Kr^{34+} cannot

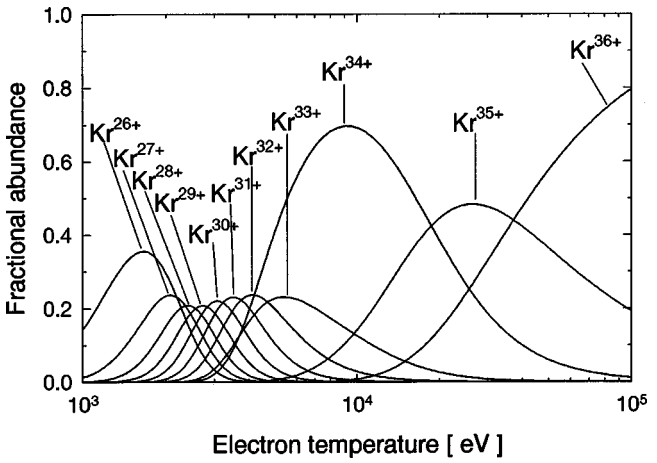

FIG. 2. Fractional abundances of the krypton ion-charge states for coronal equilibrium as a function of the electron temperature. Only the populations between Ne-like Kr^{26+} and Kr^{36+}, the terminal charge state, are shown.

reach maximum populations in excess of 20–35 %, which is in part due to the ionization potentials for these ions.

We have matched the ion abundances in EBIT to the calculated charge-state distribution by a least-squares fit. The best fit to the experimental data is obtained for the ionization balance corresponding to $kT_e = 4.7$ keV. Table I displays the ion abundances, and it can be seen that all charge states are reproduced rather well, except Li-like Kr^{33+} which is underestimated by the fit with about 25%. However, Li-like Kr^{33+} accounts only for 22% of all the krypton ions according to our calculation. Thus, relating to the relative charge-state balance, this difference translates into an uncertainty of no more than about 6%. Taking the effect from all charge states into account, the fractional difference between the two distributions in Table I is about 12%. It should not be viewed as surprising that the ion abundances in EBIT cannot be matched in an arbitrarily accurate way to the charge-state balance of a plasma. The reason is that the processes that affect the ion population in an EBIT and in a plasma are in general very different. In hot plasmas, for example, it is important to account for dielectronic recombination. Our calculations for krypton indeed suggest that the rate at which Li-like or Be-like ions recombine via dielectronic processes can dominate any other rate. For $T_e = 1$ keV, for example, the DR rate is more than two orders of magnitude larger than the ionization rate, and, although the DR rate does decrease strongly with increasing temperature, at $T_e = 5$ keV, both rates are still of equal magnitude. In EBIT, the situation is different since the electron-beam energy is normally selected such that it does not match any dielectronic resonance (in order not to deplete a particular charge state). Further, taking the nature of the EBIT into account, there are limitations on the steady-state ionization balance achievable with it due to charge-exchange recombination and ion escape from the trap. It should be noted that charge-exchange recombination is in fact one reason why we could not enhance the fraction of the He-like krypton ions to the high level existing in plasmas with temperatures above 4.7 keV.

It remains to present the relation from which the factor F, defined in Eq. (7), can be inferred from experimental data. As outlined in Sec. II, this quantity is required to provide an absolute scale for the radiative cooling-rate measurement. Inspection of Eq. (6) shows that a way of determining F is to count the x rays emitted during a specific electron-ion interaction and relate the measurement to the cross section associated with the process. In the present analysis, we rely on this procedure and make use of the intensities of the x rays produced by radiative recombination onto the $n=2$ shell. The RR $n=2$ counts can easily be separated in the experimental spectrum, and the radiative-recombination cross sections are theoretically known to a high degree of accuracy (3% error limit according to Ref. [18]). In terms of $\sigma_{\mathrm{RR}(2)}(q,E)$, the cross section for radiative recombination to $n=2$, and $I^{\mathrm{tot}}_{\mathrm{RR}(2)}$, the total number of $n=2$ radiative-recombination photons, the factor F is given by

$$F = \frac{I^{\mathrm{tot}}_{\mathrm{RR}(2)}}{W_{\mathrm{RR}}(90°)\sum_q x_q(\Lambda)\,\sigma_{\mathrm{RR}(2)}(q,E)}. \tag{10}$$

The $x_q(\Lambda)$ are the fractional ion abundances listed in Table I, and the sum is over $q=30-34$. For $\sigma_{\mathrm{RR}(2)}(q,E)$ we use the theoretical results of Behar and Doron [17], who have made detailed calculations of the cross sections using the multiconfiguration relativistic HULLAC computer code. $W_{\mathrm{RR}}(90°)$ is the angular correction factor for radiative recombination. This correction is necessary in Eq. (10) to allow for the anisotropy of the radiation intensity resulting from recombination of ions and electrons from a beam. The angular factor shows major variations as a function of the electron energy, but is fairly independent of the ion species [18]. For the beam energy (10 keV) at which we measure $I^{\mathrm{tot}}_{\mathrm{RR}(2)}$, we use $W_{\mathrm{RR}}(90°)=1.25$ [11]. Evaluating the factor F for the conditions of this experiment, we find $F = 1.93\times10^{22}$ s^{-1} cm^{-2}, with an uncertainty of about 15%.

B. Scatter plot and x-ray spectra

We now proceed with a survey of our x-ray spectroscopic measurements and show in Fig. 3(a) the scatter plot from the highly charged krypton ions produced with the technique descibed in Sec. III. The bright traces between about 1 and 4 keV x-ray energy belong to the L-shell spectra of krypton where $n=3-2$, $n=4-2$, etc. x rays are emitted subsequent to impact excitation by electrons. We emphasize here that the L-shell radiation is the dominant contributor to the cooling rate producing more than 75% of the total x-ray flux. Below 1 keV x-ray energy, the M-shell spectra of krypton are situated. The M-shell lines originate from the population of shells above $n=3$ by electron impact or recombination. Due to the particular design parameters of our solid-state detector, spectroscopic analysis of the relatively low-energy M-shell x rays could be performed down to the range of 400 eV. The traces at 13.0 and 15.5 keV x-ray energy represent direct excitation lines ($n=2-1$ and $n=3-1$ transitions) of the K-shell spectrum of krypton. X rays from radiative recombination appear as slanted bands, since their energies equal the increasing kinetic energy of the recombining electron plus the binding energy of the state it is bound to. The RR bands marked in Fig. 3(a) involve electron capture into $n=2$ and $n=3$ levels of krypton ions. In addition to these line structures, dielectronic-recombination resonances are

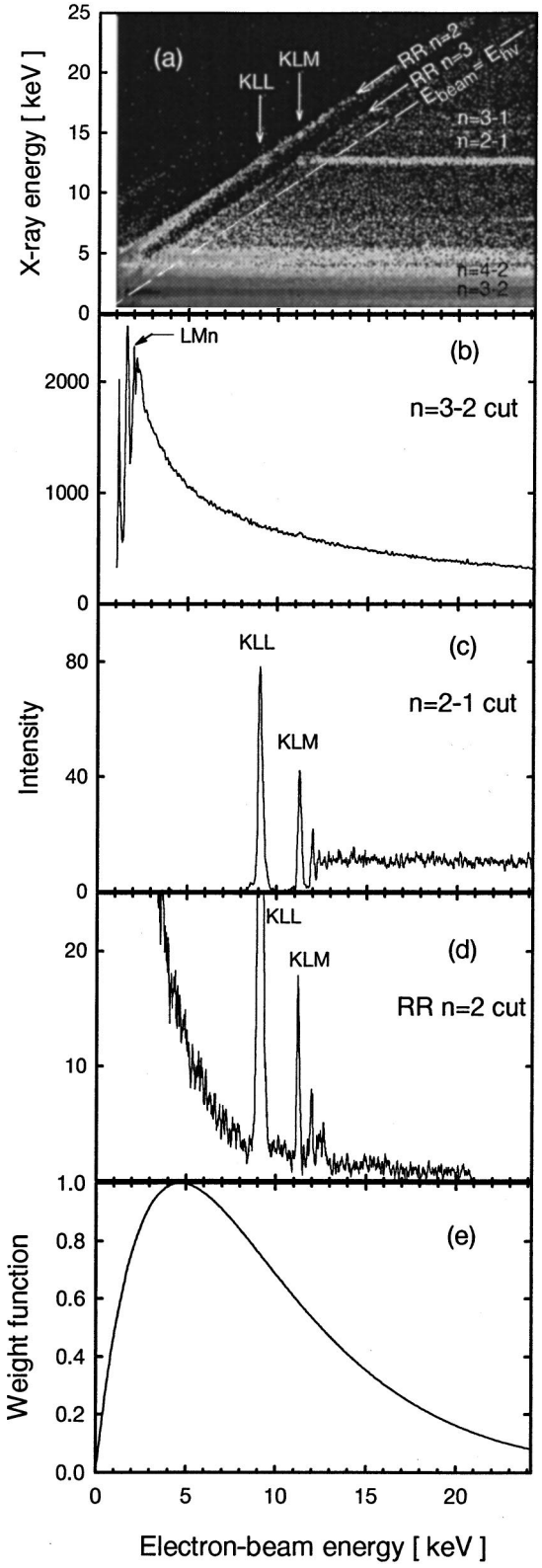

FIG. 3. (a) Scatter plot of x-ray events versus electron-beam energy for highly charged krypton ions. The trace at about 5 keV x-ray energy originates from a minor barium background in the trap. (b)–(d) Excitation curves for three separate x-ray bands. The projections (b) and (c) are from horizontal cuts along the $n=3-2$ and $n=2-1$ x-ray bands, respectively. The excitation curve (d) is from a cut along the slanted RR $n=2$ band. (e) Energy variation of the weight function [$\sqrt{E}f_e(E,T_e)$ normalized to unity] in Eq. (8) for an electron temperature of 4.7 keV.

manifested by intense spots like, for instance, the KLn ($n=2,3,\ldots$) resonance series. Note that, for $n>2$, each dielectronically excited ion can stabilize via two branches producing either a lower-energy or a higher-energy resonance. Below the line designated $E_{\rm beam}=E_{h\nu}$, where the electron-beam energy is greater than the x-ray energy, grows a background resulting from bremsstrahlung.

By applying cuts to the scatter plot and projecting the events found in these cuts onto the electron-beam energy axis, we can generate the energy-dependent excitation curves $I_{h\nu}(E)$ required for the evaluation of the cooling rates. As an example, we display in Figs. 3(b)–3(d) excitation curves for three separate x-ray bands. The $n=3-2$ cut of Fig. 3(b) contains the x rays from the collisionally excited $n=3-2$ transitions and, at the lower electron-beam energies, the dielectronic-recombination x rays from the LMN, LMO, etc. resonances. The first member of the LMn series (the LMM resonance occurring at about 750 eV resonance energy) could not be excited due to the limitations on the beam-accelerating voltage at the low end of the scan interval. Nevertheless, we have incorporated its effect in the cooling rate, too. We determined the intensity of the LMM resonance from the measured LMN dielectronic-recombination x rays by making use of the theoretical ratio of the DR resonance strengths for the LMN and LMM resonances $(S^{\rm DR}_{LMN}/S^{\rm DR}_{LMM})_{\rm theor}$. The calculations of Ref. [17] predict this ratio to be 0.6. It should be noted, however, that the LMM dielectronic-recombination term contributes only a small amount to the cooling rate, and we estimate the uncertainty added by this procedure to our overall uncertainties not to exceed 1%. The $n=2-1$ cut of Fig. 3(c) depicts the x rays from the collisionally excited $n=2-1$ transitions and the $n=2-1$ dielectronic-recombination x rays from the KLn ($n=2,3,\ldots$) resonances. The two most prominent peaks are identified and labeled KLL and KLM in the figure. Further, it may be seen from Fig. 3(c) that the higher DR members merge smoothly into the spectrum of the directly excited $n=2-1$ transitions, reflecting equal cross sections for dielectronic recombination and electron-impact excitation at the direct excitation threshold. (We recall that the threshold for exciting $n=2-1$ x-ray transitions is located at about 13 keV.) Figure 3(d) is the excitation curve for the RR $n=2$ cut, showing the higher-energy x rays from the KLn resonances and the radiative-recombination x rays from electron capture into the $n=2$ levels of krypton ions. In accordance with the approximate $1/E$ scaling of the RR cross sections [13], the intensity of the RR x rays diminishes quickly at high energy.

Once we have generated the excitation curves for the various radiation processes we can evaluate the cooling rates by taking the Maxwellian average according to the expression Eq. (8). In Fig. 3(e), we show the energy variation of the weight function in Eq. (8) visualizing that its effect is largest for $E=kT_e$ where $\sqrt{E}f_e(E,T_e)$ is at maximum. Figure 3(e) also explains why the direct excitation $n=3-2$ x rays produce large contributions to the cooling rate while the dielectronic-recombination x rays from the LMn resonances, which extend the $n=3-2$ spectra to energies below threshold, decrease rapidly in importance relative to the L-shell emission lines.

TABLE II. Rate coefficients and cooling rates for high-ionization species of krypton due to bremsstrahlung, dielectronic recombination (DR), radiative recombination (RR), and line radiation following electron-impact excitation (IE). The distribution of the krypton ion-charge states in EBIT approaches the ionization balance of a Maxwellian plasma at a temperature of 4.7 keV. The rate coefficients are given in units of 10^{-12} cm^3 s^{-1}. The cooling rates are given in units of 10^{-27} W cm^3.

Process	Channel	Rate coefficient	Cooling rate
Bremsstrahlung		0.06	0.83
DR	KLL	0.10	0.21
DR	KLM	0.05	0.11
DR	KLn $(n=N,O,\ldots)$	0.04	0.01
DR	KMn $(n=M,N,\ldots)$	0.01	0.09
DR	LMM	1.42	0.45
DR	LMN	1.25	0.46
DR	LMn $(n=O,P,\ldots)$	3.61	1.47
RR	RR $n=2$	0.69	0.98
RR	RR $n=3$	0.30	0.27
RR	RR $n=4,5,\ldots$	0.48	0.29
IE (K shell)	$n=2-1$	0.14	0.29
IE (K shell)	$n=3-1$	0.01	0.03
IE (L shell)	$n=3-2$	59.40	17.16
IE (L shell)	$n=4-2$	10.80	4.77
IE (L shell)	$n=5,6,\ldots-2$	1.71	0.98
IE (M shell)	$n=4,5,\ldots-3$	9.54	1.24
Total			29.64

C. Angular corrections

In determining the cooling rates, we have to account for the nonisotropic x-ray emission in EBIT causing intensities to vary with the angle between the electron-beam axis and the direction of observation. The angular distribution of photon emission is usually described in terms of the angular correction factor $W_\kappa(\vartheta)$, which is the ratio between the x-ray emission observed at the particular angle ϑ and its spherical average ($\vartheta=90°$ in our experiment). $W_\kappa(\vartheta)$ depends on the collision process under consideration and varies with the electron-ion interaction energy (excitation through dielectronic electron capture is an exception). In our analysis of the measured x-ray intensities, we rely on theoretical results obtained for electric dipole radiation because this type of electromagnetic interaction overwhelmingly dominates the emission from EBIT. We have calculated $W_\kappa(90°)$ for bremsstrahlung, radiative recombination, dielectronic recombination, and electron-impact excitation.

The angular correction factors for electron bremsstrahlung and radiative recombination were derived using the theoretical results of Refs. [19] and [18], respectively. Their respective energy-averaged expressions have the values $W_{\rm brems}(90°)=1.24$ and $W_{\rm RR}(90°)=1.32$. For electric dipole lines emitted during dielectronic recombination, we have calculated $W_{\rm DR}(90°)$ for a large number of individual resonances using theoretical DR cross sections from Refs. [11,17] and polarization data for He- and Be-like target ions from Ref. [20] and for Li-like ions from Ref. [21]. We infer from our results that the majority of the DR lines is enhanced relative to isotropic emission. The average of the angular correction factor for the DR lines of a resonance group is typically at the $10-15\,\%$ level. We have not calculated $W_{\rm DR}(90°)$ for B-like Kr^{31+} and C-like Kr^{30+} considering that, in the present investigation, the largest population of krypton ions is concentrated in the Be-like to He-like charge states. To treat the case of electron-impact excitation, we have used the results of Refs. [22] and [23] where collision strengths for exciting magnetic sublevels were calculated for He-like and Li-like electron configurations. According to our calculation, the largest effect occurs for the $n=2-1$ transitions where we assign a 20% correction for the x-ray intensity corresponding to $W_{n=2-1}(90°)=1.20$. For the dominant $n=3-2$ and $n=4-2$ transitions, we determined the angular correction factors to be $W_{n=3-2}(90°)=1.09$ and $W_{n=4-2}(90°)=1.06$, respectively.

It should perhaps be pointed out that the line-specific angular correction factors vary only within certain limits with changes in the relative sublevel populations. This is important because from the predicted variation we can infer the bounds of confidence of our calculated values for $W_{\rm IE}(90°)$. Conservatively, we estimate our angular correction to be accurate within a $10-20\,\%$ error interval.

V. RADIATIVE COOLING RATES

The listed cooling rates in Table II are obtained from our x-ray measurements by distinguishing between the different radiation channels. In particular, Table II contains rates for x-ray emission lines from the K-shell, L-shell, and M-shell transitions as well as from the KLn, KMn, and LMn dielectronic-recombination resonances. Also given are the rates for bremsstrahlung and electron capture into two specific levels of krypton ions. In addition, for each of the radiation channels considered, the channel-specific rate coeffi-

cient, R, is incorporated in the table. The rate coefficient is the product of the cross section associated with the collision process and the electron velocity averaged over the Maxwellian velocity distribution. It is determined by substituting the channel-specific excitation curves in Eq. (8) and performing merely the integration over E. Since we cannot resolve individual charge states in the excitation curves, the rate coefficients in Table II represent the sum over the fractional ion abundances in EBIT.

In order to assess the rates for the L-shell x-ray lines, a synthetic spectrum was fitted to the experimental data. The spectrum was modeled as a sum of separate Gaussian profiles, one for each x-ray peak. The individual rates given in Table II for the $n=3-2$ and $n=4-2$ x rays represent the fitting results for these transitions. The x rays from higher members of the L-shell spectra are completely unresolved; in Table II, solely the overall rate is given for this part of the spectrum. It is apparent from Table II that the L-shell lines make the dominant contribution to the observed x-ray flux. They radiate at a rate of 2.3×10^{-26} W cm^3, which is more than 75% of the total cooling rate. For the K-shell spectra, analysis of the emission was done for the $n=2-1$ and $n=3-1$ x rays. The K-shell lines give only minor contributions to the cooling rate, which is in part due to the energy thresholds for exciting the transitions and in part because of the lower excitation-cross sections for K-shell electrons. The M-shell lines are not resolved by our solid-state detector. They merge to a single M-shell peak in the observed spectrum. Finding the amplitude of the M-shell peak, however, was problematic because the detector efficiency varies with energy in this range. An approximation to the correct shape was determined by attaching a Gaussian profile to the M-shell peak and fitting the intensities at the high-energy side. The Gaussian fit parameters (amplitude and width) were then used to extract the size of the cooling rate for the M-shell peak.

Table II exhibits that electron-ion recombination (dielectronic and radiative) is less important as a cooling channel compared to direct excitation of L-shell electrons. Only the x rays from the LMn dielectronic resonances produce a contribution that reaches about 10% of the total cooling rate. On the other hand, it follows from the data of Table II that the total cooling rate for dielectronic recombination ($L_{\rm DR}^{\rm tot}=2.8\times10^{-27}$ W cm^3) is about two times larger than the total rate for radiative recombination ($L_{\rm RR}^{\rm tot}=1.5\times10^{-27}$ W cm^3). This result is consistent with the respective rate coefficients for dielectronic and radiative recombination. According to Table II, the total DR and RR rate coefficients have the values $R_{\rm DR}^{\rm tot}=6.5\times10^{-12}$ cm^3 s^{-1} and $R_{\rm RR}^{\rm tot}=1.5\times10^{-12}$ cm^3 s^{-1}, showing that recombination via dielectronic processes occurs about four times more frequently than radiative recombination. As a check on the reliability of our atomic data for the calculation of the ionization balance, we have compared the experimental results for $R_{\rm DR}^{\rm tot}$ and $R_{\rm RR}^{\rm tot}$ to the values we derived from our ionization-equilibrium calculations. For $kT_e=4.7$ keV, we determine $(R_{\rm DR}^{\rm tot})_{\rm theor}=5.5\times10^{-12}$ cm^3 s^{-1} and $(R_{\rm RR}^{\rm tot})_{\rm theor}=1.2\times10^{-12}$ cm^3 s^{-1}, which agrees with the experimental result within a 20% error limit, and thus confirms the DR and RR rate coefficients used in the present analysis.

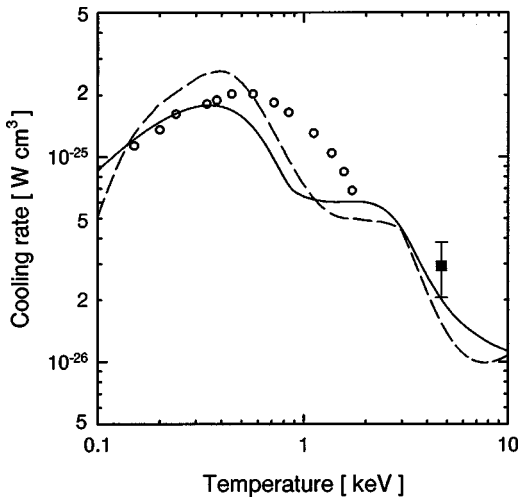

FIG. 4. Radiative cooling rate for krypton as a function of the electron temperature. The solid curve represents the *ab initio* HULLAC calculation by Fournier *et al.* [8] and the broken curve the average-ion model calculation by Post *et al.* [7]. The result at $kT_e=4.7$ keV is from the present EBIT experiment. The data points below about 2 keV are from recent krypton experiments at the Frascati Tokamak Upgrade FTU [9].

For our measurement of the cooling rate, we estimate an uncertainty interval of $22-30\%$. We calculated the total uncertainty by adding all the individual errors in quadrature. The largest uncertainties are in the calculation of the angular corrections ($10-20\%$ error) and the determination of the F factor according to Eq. (10) (15% error). Another source of error arises from the change of the detector efficiency for incident x-ray energies below 1 keV (5% error) and from the statistical uncertainties (1% error). One possible cause of systematic error is additional counts from background ions (barium) overlapping the L-shell spectra of krypton. We made some measurements without injecting krypton to secure an independent assessment of the x radiation from barium ions. From the results, we infer that the effect of a possible contamination of the L-shell x rays adds a systematic uncertainty of no more than 3% to the determination of the cooling rate.

In Fig. 4, we compare the experimental total cooling rate to the values predicted by two different models. The calculation by Post *et al.* [7] is based on the averaged-ion model, while Fournier *et al.* [8] use *ab initio* atomic data calculated with the HULLAC package. Also shown are the results from the recent krypton experiment at the FTU [9]. One immediate conclusion is that the cooling rate of the present work is in disagreement with both calculations. It differs from the predicted values by a factor of $1.5-2$, depending on the theoretical model. We attribute the difference between measurement and calculation to the power lost through the L-shell radiation of krypton. It turns out that this contribution is underestimated in the theoretical treatment. However, it is also seen in the figure that the HULLAC curve [8] touches the 30% error limit of our measurement indicating that this calculation provides a better estimate of the cooling rate than the older model [7].

VI. CONCLUSIONS

We have measured the radiative cooling rates for high-ionization species of krypton using the EBIT facility. The

measurements employ a technique where a steady-state ion population in EBIT is probed by fast scans of the beam energy. For the present investigation, the EBIT was tuned to a charge-state distribution approaching the ionization balance of a plasma at a temperature of 4.7 keV. The fractional abundances of the highly charged krypton ions were determined from the *KLL* dielectronic-excitation spectrum following the procedure described in Ref. [11]. For the conditions of this experiment, C-like Kr^{30+} to He-like Kr^{34+} ions were detected in the trap. To determine the cooling rate, the trapped ions were sampled over a scan interval extending from 0.9 to 25 keV, and spectroscopic analysis of the emitted radiation was done from about 400 eV to the 25-keV x ray range. We made use of EBIT's capabilities to distinguish between different electron-ion interactions and have measured the x-ray emission from bremsstrahlung, radiative recombination, dielectronic recombination, and line radiation following electron-impact excitation.

Our EBIT measurement has the advantage over experiments on tokamak plasmas that it is channel specific and that no integration over a range of electron temperatures and densities occurs. Such measurements reveal more details of the radiation rates and indicate what fraction of the total x-ray flux proceeds via which of the different radiation channels. For $T_e = 4.7$ keV, the dominant contribution to the cooling rate is made by the $n = 3-2$, $n = 4-2$, ... x rays of the *L*-shell spectra of krypton, which produce more than 75% of the total radiation loss. For the total cooling rate, a difference is noted between the measurement and theoretical calculations. The predicted values are lower by a factor of $1.5-2$, depending on the theoretical model. For the experimental cooling rate, we estimate the uncertainty interval to be $22-30\,\%$.

In the present EBIT measurement, we have obtained radiative cooling rates for one particular charge-state distribution. By performing x-ray spectroscopic measurements for several different $x(\Lambda)$ distributions, which need not necessarily approach a specific $x(T_e)$ distribution, and summing weighted spectra, our procedure represents a way of constructing cooling rates for a range of plasma temperatures. The weights are then to be determined from an ionization-recombination model of the plasma.

[1] S. A. Cohen, K. A. Werly, D. E. Post, B. J. Braams, J. L. Perkins, and D. Pearlstein, J. Nucl. Mater. **176&177**, 909 (1990).

[2] C. J. Cummings, S. A. Cohen, R. Hulse, D. E. Post, M. Redi, and J. Perkins, J. Nucl. Mater. **176&177**, 916 (1990).

[3] M. Bitter, H. Hsuan, C. Bush, S. Cohen, C. J. Cummings, B. Grek, K. W. Hill, J. Schivell, M. Zarnstorff, P. Beiersdorfer, A. Osterheld, A. Smith, and B. Fraenkel, Phys. Rev. Lett. **71**, 1007 (1993).

[4] M. Bitter, H. Hsuan, K. W. Hill, R. Hulse, M. Zarnstorff, and P. Beiersdorfer, in *Atomic and Plasma-Material Interaction Processes in Controlled Thermonuclear Fusion*, edited by R. K. Janev and H. W. Drawin (Elsevier Science, Amsterdam, 1993), p. 119.

[5] K. W. Hill, S. D. Scott, M. Bell, R. Budny, C. E. Bush, R. E. H. Clark, B. Denne-Hinnov, D. R. Ernst, G. W. Hammett, D. R. Mikkelsen, D. Mueller, J. Ongena, H. K. Park, A. T. Ramsey, E. J. Synakowski, G. Taylor, M. C. Zarnstorff, and the TFTR Group, Phys. Plasmas **6**, 877 (1999).

[6] K. Widmann, P. Beiersdorfer, V. Decaux, R. Elliott, D. Knapp, A. Osterheld, M. Bitter, and A. Smith, Rev. Sci. Instrum. **66**, 761 (1995).

[7] D. E. Post, R. V. Jensen, C. B. Tarter, W. H. Grasberger, and W. A. Lokke, At. Data Nucl. Data Tables **20**, 397 (1977).

[8] K. B. Fournier, M. J. May, D. Pacella, B. C. Gregory, J. E. Rice, J. L. Terry, M. Finkenthal, and W. H. Goldstein, in *Atomic Processes in Plasmas 11th Topical Conference*, edited by E. Oks and M. Pindzola, AIP Conf. Proc., **443**, (AIP, Woodbury, NY, 1998), p.73.

[9] M. J. May, M. Finkenthal, V. Soukhanovskii, D. Stutman, H. W. Moos, D. Pacella, G. Mazzitelli, K. Fournier, W. Goldstein, and B. Gregory, Rev. Sci. Instrum. **70**, 375 (1999).

[10] C. Breton, C. De Michelis, and M. Mattioli, J. Quant. Spectrosc. Radiat. Transf. **19**, 367 (1978).

[11] T. Fuchs, C. Biedermann, R. Radtke, E. Behar, and R. Doron, Phys. Rev. A **58**, 4518 (1998).

[12] W. Lotz, Z. Phys. **216**, 241 (1968).

[13] Y. S. Kim and R. H. Pratt, Phys. Rev. A **27**, 2913 (1983).

[14] Y. Hahn, J. Quant. Spectrosc. Radiat. Transf. **49**, 81 (1993).

[15] Y. Hahn, J. Quant. Spectrosc. Radiat. Transf. **51**, 663 (1994).

[16] I. P. Grant, B. J. McKenzie, P. H. Norrington, D. F. Mayers, and N. C. Pyper, Comput. Phys. Commun. **21**, 207 (1980).

[17] E. Behar and R. Doron (private communication).

[18] J. H. Scofield, Phys. Rev. A **40**, 3054 (1989).

[19] H. K. Tseng, R. H. Pratt, and C. M. Lee, Phys. Rev. A **19**, 187 (1979).

[20] M. K. Inal and J. Dubau, J. Phys. B **22**, 3329 (1989).

[21] A. S. Shlyaptseva, R. C. Mancini, P. Neill, P. Beiersdorfer, J. R. Crespo López-Urrutia, and K. Widmann, Phys. Rev. A **57**, 888 (1998).

[22] M. K. Inal and J. Dubau, J. Phys. B **20**, 4221 (1987).

[23] H. L. Zhang, D. H. Sampson, and R. E. H. Clark, Phys. Rev. A **41**, 198 (1990).